INSTITUT DE FRANCE
Académie des sciences

Comptes Rendus
Mécanique

A. David V. Brou and Aya Brigitte N'Dri

Evaluation of an optimized bush fire propagation model with large-scale fire experiments

Volume 349, issue 1 (2021), p. 43-53

Published online: 4 March 2021

https://doi.org/10.5802/crmeca.77

Les Comptes Rendus. Mécanique *sont membres du Centre Mersenne pour l'édition scientifique ouverte*
www.centre-mersenne.org
e-ISSN : 1873-7234

Comptes Rendus
Mécanique
2021, 349, nº 1, p. 43-53
https://doi.org/10.5802/crmeca.77

Short paper / *Note*

Evaluation of an optimized bush fire propagation model with large-scale fire experiments

A. David V. Brou[*, a] **and Aya Brigitte N'Dri**[b]

[a] Université Jean Lorougnon Guédé de Daloa, UFR Environnement, Laboratoire des Sciences et Technologies de l'Environnement, BP 150 Daloa, Côte d'Ivoire

[b] Université Nangui Abrogoua, UFR des sciences de la nature, Laboratoire d'Ecologie et Développement Durable, Station d'Ecologie de Lamto/CRE, Côte d'Ivoire

E-mails: brou.akahoua@ujlg.edu.ci (A. D. V. Brou), ndri.brigitte@yahoo.fr (A. B. N'Dri)

Abstract. Thirty-one bush fire experiments are used to assess the predictive capability of a bush fire spread model. This model has been optimized by a deterministic method of parameter calibration. The experiments used were carried out each year from 2014 to 2017 in a forest–savannah transition zone. The characteristics of the herbaceous stratum as well as the meteorological and topographical data are well documented. The characteristics of the fire have also been measured to understand the behaviour of the fire in a Guinean savannah. The predicted rate of fire spread and fire contours gave results in good accordance with those of the experiments.

Résumé. Trente et une (31) expériences de feu de brousse ont été utilisées pour évaluer la capacité prédictive d'un modèle de propagation de feux de brousse. Ce modèle a été optimisé par une méthode déterministe de calibrage des paramètres. Les expériences utilisées ont été réalisées chaque année de 2014 à 2017 dans une zone de transition forêt - savane. Les caractéristiques de la strate herbacée ainsi que les données météorologiques et topographiques ont été bien documentées. Les caractéristiques du feu ont été également mesurées pour comprendre le comportement du feu dans une savane Guinéenne. Les vitesses de propagation et les contours de feux prédits ont donné des résultats en bon accord avec ceux des expériences.

Keywords. Optimized model evaluation, Calibration parameter, Large-scale bush fire experiments, Rate of spread, Fire propagation, Guinean savannah.

Manuscript received 8th December 2020, revised 30th January 2021, accepted 3rd February 2021.

1. Introduction

Global warming has contributed to the increase in the number of forest fires in the world. Africa is no exception to this phenomenon. In August 2019, satellite images from the National Aeronautics

* Corresponding author.

and Space Administration (NASA) revealed that some fire severity similar to that of the Amazon rainforest affect sub-Saharan Africa [1].

Bush fires have aftermaths on forests, on the environment through global change and warming and on living beings: loss of human life, animal, and plant species destruction.

In order to prevent or mitigate such events, it is necessary to obtain reliable models that are able to predict the spatial progression of fire. These models are needed as well for tactical fire control and management, for personnel training as for prevention.

A safe and an effective control of wildfires and the use of fire as a management tool depend on the ability to predict fire behaviour as accurately as possible [2].

While detailed physical fire models are still not suitable for forest fire emergencies, the so-called operational semi-physical models are unable to provide accurate estimates of macroscopic fire behaviour [3, 4].

Bush fires are complex phenomena and their modelling suffer both from a lack of knowledge of the detailed physics of the processes involved and a large amount of input data required by the models [5, 6].

Parameter estimation in environmental modelling is essential for input parameters, which are difficult or impossible to measure. Especially in simulations for disaster propagation prediction, where hard real time constraints must be respected in order to avoid tragedy [7].

For few years, efforts have been undertaken to improve model predictions and reduce their uncertainties.

In this paper, we are going to test a semi-physical model of vegetation fire propagation, optimized by calibrating its parameters [8]. This model is classified among the so-called network models. Initially developed by Porterie *et al.* [9–12], it has undergone several protrusions to become a semi-physical model [13, 14]. In the last model phenomena that occur at the macroscopic scale are taken into account. These include the preheating of fuel bed by flame radiation and by convection of hot gases, but also its cooling by radiative exchange with the surrounding environment.

In order to evaluate the model's ability to predict real fires, thirty-one large-scale fire experiments were simulated. These experiments took place in the Guinean savannah of the Lamto reserve in Côte d'Ivoire. The different experiment sites are located in a forest–savannah transition zone. Every year in northern Côte d'Ivoire, bush fires destroy plantations and cause loss of human life [15].

The article is organized as follows. First, we briefly describe the general concepts and physical approach of the model then the optimization method. Second, we present the large-scale fire experiments used to test the model. Third, we compare the results of the model with those of the experiments. Finally, in the last section, conclusions are drawn.

2. Model description and optimization method

2.1. *Presentation of the model*

In this section, we briefly present the model. For more details see [8].

The combustible layer, in the model, is divided into cells of equal size. A burning cell transfers heat to healthy cells (Figure 1). A combustible cell j is said to be healthy when its temperature T_j is equal to the ambient temperature T_∞. The energy absorbed by the combustible cell when it is exposed to the fire front is used to raise the temperature of wet fine fuel elements to the boiling temperature of water, 373 K, evaporate the moisture, and raise the temperature of dry fine fuel elements to the ignition temperature T_{ign}. The combustible cell then continues to burn with a flame, while transferring heat to the neighbouring cells by means of convection and radiation.

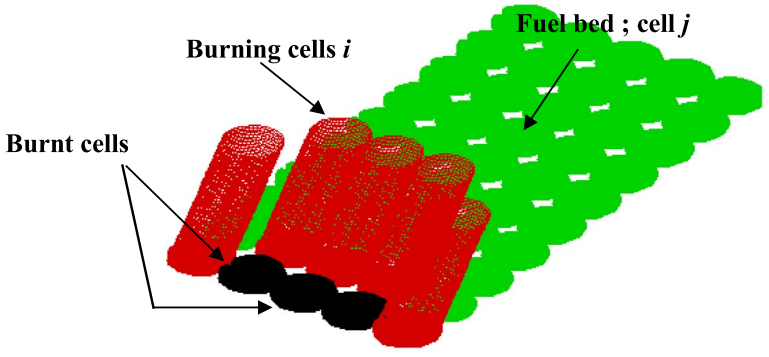

Figure 1. Solid flame model and schematic of the network showing burning cells, burnt cells, and healthy cells.

In the solid flame model, the visible flame is regarded as a uniformly radiating solid body with a cylindrical shape and with thermal radiation emitted from its surface.

The total energy q_j absorbed by cell j is used on the one hand to raise the temperature of fine fuel elements and on the other hand to evaporate moisture at the boiling temperature of water

$$q_j = \begin{cases} \rho_j C_{pj} \phi_j \dfrac{\mathrm{d}T_j}{\mathrm{d}t}, & \text{for } T_j \neq 373 \text{ K} \\ -\rho_j h_{\text{vap}} \phi_j \dfrac{\mathrm{d}W_j}{\mathrm{d}t}, & \text{for } T_j = 373 \text{ K}, \end{cases} \tag{1}$$

where T_j and W_j are, respectively, the mean temperature and the mass fraction of water of cell j, ρ_j is the fuel-particle density, C_{pj} is the specific heat capacity, h_{vap} is the specific enthalpy change of water to vapour at 373 K, and ϕ_j is the packing ratio.

Let N_j be the number of burning cells that interact with cell j, we have

$$q_j = \sum_{i=1}^{N_j} q_{ij}, \tag{2}$$

where q_{ij} is the total heat flux emitted from the burning cell i which is received by cell j. It is the sum of all possible heat transfer mechanisms: radiation on the top surface of cell j, internal radiation from the ember zone, convection on the top surface of cell j, internal convection inside the fuel bed, radiation loss to the ambient at the top surface of cell j, and is given by the following relation:

$$\begin{aligned} q_{ij} = {} & \underbrace{\frac{a_{\text{fb}} \varepsilon_{\text{fl}} \sigma T_{\text{fl}}^4}{H_j} F_{ij}}_{\substack{\text{surface} \\ \text{radiation}}} + \underbrace{0.25 A_{\text{fb}} \varepsilon_b \sigma T_b^4 \exp(-0.25 A_{\text{fb}} d_{ij})}_{\substack{\text{internal} \\ \text{radiation}}} \\ & + \underbrace{\frac{0.565 k_{\text{fl}} Re_{d_{ij}}^{1/2} Pr^{1/2}}{d_{ij} H_j} (T_{\text{fl}} - T_j) \exp(-0.3 d_{ij}/L_{\text{fl}}) \beta_{ij}}_{\substack{\text{surface} \\ \text{convection}}} \\ & + \underbrace{\frac{0.911 A_{\text{fb}} k_b Re_D^{0.385} Pr^{1/3}}{\text{diam}_j} (T_b - T_j) \exp(-0.25 A_{\text{fb}} d_{ij}) \beta_{ij}}_{\substack{\text{internal} \\ \text{convection}}} - \underbrace{\frac{\varepsilon_{\text{fb}} \sigma (T_j^4 - T_\infty^4)}{H_j}}_{\substack{\text{radiative} \\ \text{loss}}}. \end{aligned} \tag{3}$$

The flame emissivity $\varepsilon_{\text{fl}} = 1 - \exp(-0.6L_{\text{fl}})$, where L_{fl} is the flame length, a_{fb} is the fuel-bed absorptivity, and $\sigma(= 5.67 \times 10^{-8}$ W/m^2/K) is the Stefan–Boltzmann constant. F_{ij} is the view factor, ε_b is the ember emissivity, k_b its thermal conductivity and T_b its temperature. A_{fb} is the total fuel-particle surface area per fuel-bed volume. ε_{fb} is the fuel-bed emissivity and d_{ij} is the distance between cell i and cell j. H_j is the height of the vegetative cell j. Pr is the Prandtl number and $Re_{d_{ij}}$ is the Reynolds number based on the length scale d_{ij}. k_{fl} and T_{fl} are, respectively, the thermal conductivity and the flame temperature. Re_{D_j} is the Reynolds number based on the branch diameter diam$_j$ as length scale. β_{ij} is a coefficient which is equal to unity when the straight line connecting cells i and j is aligned with the wind direction, and zero otherwise.

The model allows to describe the rate of spread and the fire contour through the evolution of temperature T_j of cells j given by (1). Taking relation (2) into account, this equation can be rewritten for $T_j \neq 373$ K as

$$\begin{cases} \dfrac{\mathrm{d}T_j}{\mathrm{d}t} = \displaystyle\sum_{i=1}^{N_j} S_{ij}(T_j(t)) \\ T_j(0) = T_\infty, \end{cases} \tag{4}$$

where

$$S_{ij} = \frac{1}{\rho_j C_{pj} \phi_j} q_{ij} \tag{5}$$

with q_{ij} given by (3).

2.2. *Optimization method*

In this section, the optimization method for calibrating the parameters is presented.

The expression of S_{ij} in (5) depends not only on the temperature T_j, but also on a set of parameters.

Let θ be the vector whose components are the parameters whose values are known with uncertainty. For our model, we have

$$\theta = (a_{\text{fb}}, T_{\text{fl}}, \varepsilon_b, \varepsilon_{\text{fb}}, k_{\text{fl}}, k_b, T_b)^T. \tag{6}$$

According to several authors in the literature (see for example [16, 17]), the fuel-bed absorptivity a_{fb} varies between [0.3; 1]. The flame temperature T_{fl} varies in the range [700; 1200]. This is in accordance with the flame temperatures measured in our experiments. The temperature of the embers T_b is taken equal to the ignition temperature and varies in the range [500; 700]. Its thermal conductivity k_b and emissivity ε_b vary respectively in the interval [0.0205; 0.105] and [0.1; 1] [18–23]. The fuel-bed emissivity varies in the same interval as that of the ember. The thermal conductivity of the flame is assumed to be those of air at the flame temperature and varies in the interval [0.0371; 0.225] [14].

Therefore, the physically admissible set $\Omega \subset \mathbb{R}^7$ in which θ varies is given by

$$\Omega = [0.3; 1] \times [700; 1200] \times [0.1; 1] \times [0.1; 1] \times [0.0371; 0.225] \times [0.0205; 0.105] \times [500; 700]. \tag{7}$$

The term S_{ij} in (5) can be rewritten using the components of θ as follows:

$$S_{ij}(\theta, T_j) = \underbrace{A_{ij}\theta_1\theta_2^4}_{\substack{\text{surface} \\ \text{radiation}}} + \underbrace{B_{ij}\theta_3\theta_7^4}_{\substack{\text{internal} \\ \text{radiation}}} + \underbrace{D_{ij}\theta_5(\theta_2 - T_j)}_{\substack{\text{surface} \\ \text{convection}}} + \underbrace{E_{ij}\theta_6(\theta_7 - T_j)}_{\substack{\text{internal} \\ \text{convection}}} - \underbrace{C_{ij}\theta_4(T_j^4 - T_\infty^4)}_{\substack{\text{radiative} \\ \text{loss}}}, \tag{8}$$

where

$$\begin{cases} A_{ij} = \dfrac{\varepsilon_{\text{fl}}\sigma}{\rho_j C_{pj}\phi_j H_j} F_{ij}; \quad B_{ij} = \dfrac{0.25 A_{\text{fb}}\sigma \exp(-0.25 A_{\text{fb}} d_{ij})}{\rho_j C_{pj}\phi_j}; \quad C_{ij} = \dfrac{\sigma}{\rho_j C_{pj}\phi_j H_j} \\ D_{ij} = \dfrac{0.565 Re_{d_{ij}}^{\frac{1}{2}} Pr^{\frac{1}{2}}}{\rho_j C_{pj}\phi_j d_{ij} H_j} \exp\left(-\dfrac{0.3 d_{ij}}{L_{\text{fl}}}\right)\beta_{ij}; \quad E_{ij} = \dfrac{0.911 A_{\text{fb}} Re_D^{0.385} Pr^{1/3}}{\rho_j C_{pj}\phi_j \text{diam}_j} \exp(-0.25 A_{\text{fb}} d_{ij})\beta_{ij}. \end{cases} \tag{9}$$

The system (4) giving the evolution of the temperature T_j can be rewritten in the following form

$$\begin{cases} \dfrac{\mathrm{d}T_j}{\mathrm{d}t} = \displaystyle\sum_{i=1}^{N_j} S_{ij}(\theta, T_j) \\ T_j(0) = T_\infty. \end{cases} \tag{10}$$

Suppose we know the position of real fire contour in a given time t_n. For a good prediction, one should have $T_j(t_n) = T_{\text{ign}}$ at t_n. Where $T_j(t_n)$ is healthy cells j temperature, which are aligned with the real contour of the fire at t_n, and T_{ign} the ignition temperature.

The aim of the optimization method is to determine the vector $\theta \in \Omega$ which carrying out at this instant, the predicted fire contour matches the best to the experimental contour. That comes to determining for all the cells of the contour, the set of parameters that minimize the difference between the two temperatures

$$\min_{\theta\in\Omega} \sum_{j=1}^{M_c} (T_j(\theta, t_n) - T_{\text{ign}})^2, \tag{11}$$

where M_c is the number of cells aligned on the real fire contour.

The temperature $T_j(\theta, t_n)$ is approximated by $T_j^{(n)}(\theta)$ obtained from (10) by solving the following fourth-order Runge–Kutta scheme

$$\begin{cases} T_j^{(n-1,2)} = T_j^{(n-1)} + \dfrac{\Delta t}{2} \displaystyle\sum_{i=1}^{N_j} S_{ij}(\theta, T_j^{(n-1)}) \\ T_j^{(n-1,3)} = T_j^{(n-1)} + \dfrac{\Delta t}{2} \displaystyle\sum_{i=1}^{N_j} S_{ij}(\theta, T_j^{(n-1,2)}) \\ T_j^{(n-1,4)} = T_j^{(n-1)} + \Delta t \displaystyle\sum_{i=1}^{N_j} S_{ij}(\theta, T_j^{(n-1,3)}) \\ T_j^{(n)} = T_j^{(n-1)} + \dfrac{\Delta t}{6} \displaystyle\sum_{i=1}^{N_j} (S_{ij}(\theta, T_j^{(n-1)}) + 2S_{ij}(\theta, T_j^{(n-1,2)}) + 2S_{ij}(\theta, T_j^{(n-1,3)}) + S_{ij}(\theta, T_j^{(n-1,4)})). \end{cases} \tag{12}$$

In (12), $T_j^{(n-1)}$ is the approximation of the temperature of cell j at times t_{n-1} and Δt is the constant time step of discretization.

From (12), we can by induction express the temperature $T_j^{(n)}$ with respect to the initial temperature T_∞, that is,

$$T_j^{(n)} = T_\infty + \frac{\Delta t}{6} \sum_{l=1}^{n-1} \sum_{i=1}^{N_j} (S_{ij}(\theta, T_j^{(l)}) + 2S_{ij}(\theta, T_j^{(l,2)}) + 2S_{ij}(\theta, T_j^{(l,3)}) + S_{ij}(\theta, T_j^{(l,4)})). \tag{13}$$

Finally, the optimization problem is

$$\min_{\theta\in\Omega} \sum_{j=1}^{M_c} \left(T_\infty + \frac{\Delta t}{6} \sum_{l=1}^{n-1} \sum_{i=1}^{N_j} (S_{ij}(\theta, T_j^{(l)}) + 2S_{ij}(\theta, T_j^{(l,2)}) + 2S_{ij}(\theta, T_j^{(l,3)}) + S_{ij}(\theta, T_j^{(l,4)})) - T_{\text{ign}} \right)^2. \tag{14}$$

A "Nonlinear Least Squares" algorithm, provided by Scilab-6.0.1 [24], is used to solve the optimization problem of relation (14).

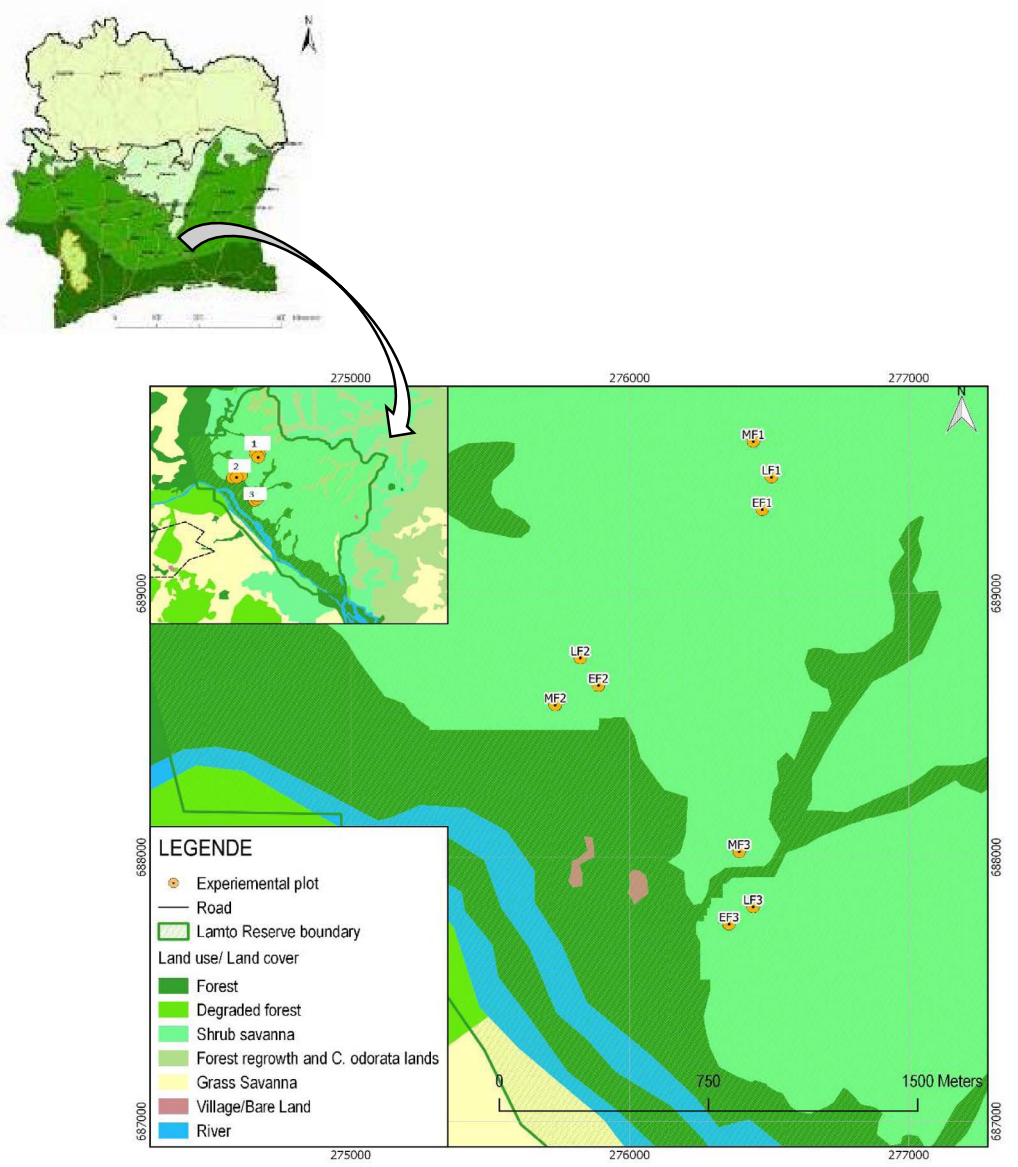

Figure 2. Location of the study site and distribution of plots in the landscape. 1, 2, and 3: experimental blocks. MF1, LF1, and EF1: mid-season fire, late-season fire, and early-season fire plots in block 1, respectively.

3. Large-scale experimental burns

The current work used data collected during thirty-one large-scale experimental burns, conducted by N'Dri *et al.* [25]. They analysed fire behaviour in the Guinean savannah of Lamto (Côte d'Ivoire) during a four-year field experiment (Figure 2).

This study was conducted on three 230 m × 120 m blocks of shrubby savannah, each separated from the surrounding similar savannah by a 10 m wide firebreak, and distant from each other by a few kilometres. Each block was divided into three 100 m × 50 m plots separated from each other

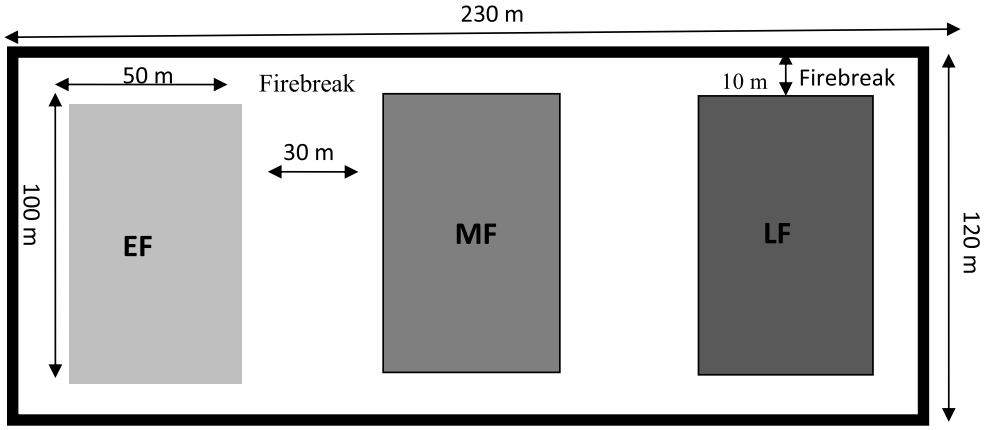

Figure 3. Experimental setup. EF is early-season fire; MF is mid-season fire; LF is late-season fire.

Table 1. Ranges of fuel characteristics, and weather parameters for the 2014–2017 period

Parameter	Range	Units
Dry fine fuel density	227.5	($kg{\cdot}m^{-3}$)
Fuel load	1.103–2.741	($kg{\cdot}m^{-2}$)
Fuel water content	19.28–48	(%)
Fuel-bed depth	0.99–2.71	(m)
Wind speed	0.3–4.46	($m{\cdot}s^{-1}$)
Air temperature	23–41.7	(°C)
Air humidity	21–75	(%)
Slope	0	(rad)

by 30 m wide firebreaks. Each plot in a block received one of three fire treatments in a full factorial design: (1) early-season fire at the start of the long dry season (~18 November); (2) mid-season fire at the middle of the long dry season (~18 January); and (3) late-season fire at the very end of the long dry season (~15 March) (Figure 3). On each plot, the designated fire treatment was applied four times from 2014 to 2017. All blocks were located on flat ground.

Fuel consisted primarily of grass and tree leaf litter. Fuel characteristics were described by the following variables before fires were applied: fuel load ($kg{\cdot}m^{-2}$), moisture content (%), and grass height (m). Fuel was collected on ten 1 m^2 quadrats per plot shortly (min) before burning. Fuel was separated into litter (fallen dead grass and tree leaves) and standing fuel (standing grass and stems), and immediately weighed for fresh mass. Samples were oven-dried at 80 °C to constant weight and weighed for dry mass. Moisture content was then calculated. Grass cover height (m) was determined as the average vertical distance from the ground to the tip of the shoot of 50 randomly selected points.

Fire was ignited with a dry palm leaf along the shorter side of each plot in the direction of the wind to rapidly establish a fire line and ensure linear ignition (Figure 4).

All burns were conducted in the morning (1000 to 1100 h) on the same day, in order to ensure similarity of fuel moisture levels and weather conditions (e.g, wind, air humidity, and temperature). Data of fuel characteristics and weather conditions are presented in Table 1.

The rate of spread was determined by using stop watches to record the time it took for a flame line to reach poles positioned every 10 m on both sides of each plot.

Figure 4. Fire start during the experiment.

4. Results

The experimental rates of spread and fire contours are compared to those predicted before and after optimization of the model.

The experiments described above have been simulated by the fire propagation model. The experimental rates of fires spread were compared to those predicted before and after optimization of the model.

Figure 5 shows the comparison between predicted and experimental fires rate of spread. On the x-axis are the experimental rates and on the y-axis are the predicted rates. The distance of the scatterplot from the linear line measures the error of the model. On Figure 5a, rate of spread is predicted with initial parameters of the model and on Figure 5b with calibrated parameters. With the initial parameters, the whole point cloud is below the linear line. Predicted rate of spread is therefore lower than that observed. On the other hand, with calibrated parameters, the points are in majority on the linear line. Consequently, prediction with initial parameters underestimates rate of spread of the head fire front. With calibrated parameters, rate of fire spread is well predicted by the model.

The results observed above are also confirmed by Figure 6. This figure shows the relative error on the fire rates of spread, predicted with the initial parameters and with the calibrated parameters.

With the calibrated parameters, twenty-three rate of fire spread were predicted with a relative error of less than 10%, two were predicted with a relative error between 10% and 15% and six were predicted with a relative error between 15% and 40%.

With the initial parameters, only six fire spread rates were predicted with a relative error of less than 40%.

The contours of six experimental fires selected were compared with those predicted with the calibrated parameters. These are the LF1 in 2014, EF2 in 2015, LF3 in 2015, LF3 in 2016, EF3 in 2017, and LF2 in 2017 experiments. The contours of these six experimental fires were well determined. For experiment LF1 in 2014, the fire contour predicted by our model is that of 324s

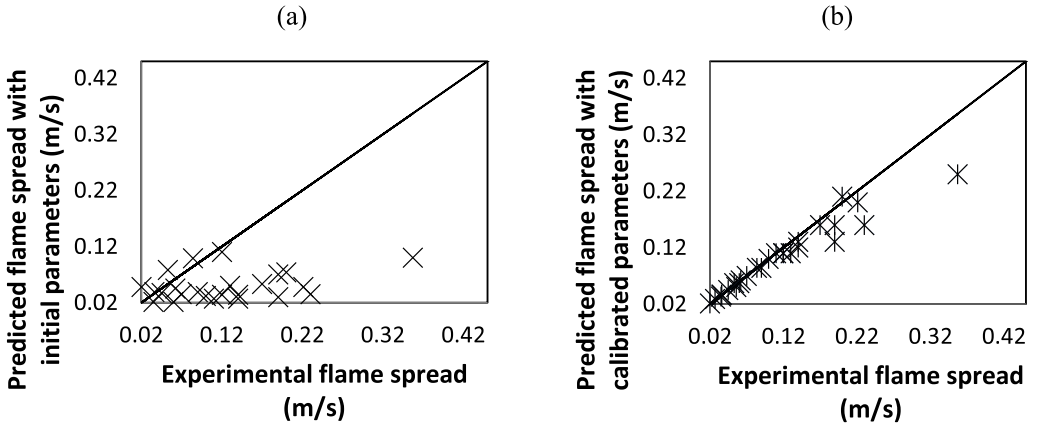

Figure 5. Comparison between experimental and predicted flame spreads with initial parameters (a) and calibrated parameters (b).

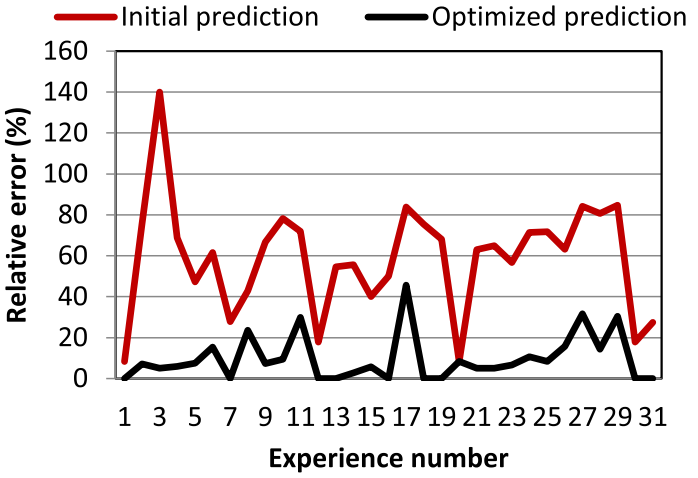

Figure 6. Relative errors between predicted and experimental flame spread. The relative error is calculated as the ratio of the absolute difference between measured (M) and predicted (P) values divided by the measured value, time 100 : $(|M-P|/M) \times 100$.

after fire start. For experiment EF2 in 2015, it is the fire contour after 2059s of propagation, 1290s for experiment LF3 in 2015, 378s for experiment LF3 in 2016, 501s for experiment EF3 in 2017 and 298s for experiment LF2 in 2017. They are compared with those predicted by the model using the input values given in Table 2.

Figure 7, compares the fire contours predicted by our model with those observed. Observing Figure 7, the agreement for the fire contour is good. The average rate of spread of the head fire front of experiments EF2 in 2015 and LF3 in 2015 is slightly overestimated. If the model slightly underestimates the spread of the head fire of experiment LF2 in 2016, the flank fire spread rate is much more so. Indeed, the contour of the experimental flank fire has reached the firebreaks and is no longer visible. This is not the case of the simulated fire contour.

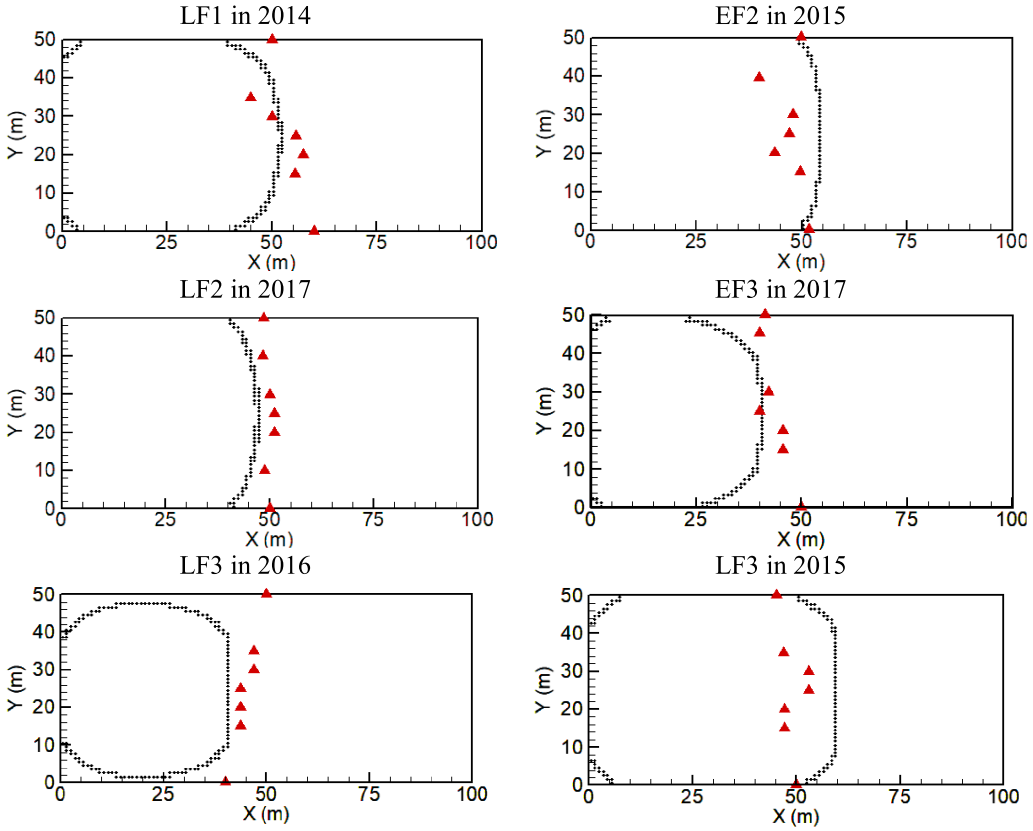

Figure 7. Comparison between predicted (black line) and observed (red symbol) fire contour for six selected experiments: LF1 in 2014, EF2 in 2015, LF2 in 2017, EF3 in 2017, LF3 in 2016, and LF3 in 2015.

Table 2. Input variables for fire spread model contours simulation

Experiment	LF1 in 2014	EF2 in 2015	LF3 in 2015	LF3 in 2016	EF3 in 2017	LF2 in 2017
Inputs						
Dry fine fuel density ($kg{\cdot}m^{-3}$)	227.5	227.5	227.5	227.5	227.5	227.5
Fuel load ($kg{\cdot}m^{-2}$)	2.03	2.43	1.63	1.37	1.94	1.39
Fuel water content (%)	26	39	40	22	37	24
Fuel-bed depth (m)	1.65	2.24	1.57	1.33	2.3	1.1
Wind speed ($m{\cdot}s^{-1}$)	2.9	0.3	2.9	4.46	1.2	0.37
Ambient temperature (k)	309	306	309	314	311	309
Flame length (m)	2.88	1.68	1.87	2.76	2.64	2.89

5. Conclusion

A simple optimized bush fire propagation model has been evaluated. This model is based on energy conservation and heat transfer between the fire front, vegetation, and ambient air. The optimization of the model is achieved by a deterministic optimization method, which allowed the calibration of the seven model parameters. Thirty-one large-scale bush fire experiments,

carried out at the Lamto reserve in Côte d'Ivoire, have been simulated. The fire spread rate and fire contour predicted by our model have been compared to the results of the experiments. The predicted rate of spread with the initial parameters underestimated those experiments. With the calibrated parameters, a good agreement has been found on both the spread rates and the fire contours.

References

[1] NASA, "Fire : 2019-08-25 and 2019-08-26", NASA. August 25, 2019. Available at: https://firms.modaps.eosdis.nasa.gov/map/#z:3;c:28.1,-17.3;t:adv-points;d:2019-08-25..2019-08-26;l:firms_noaa20-viirs,firms_viirs,firms_modis_a,firms_modis_t. Accessed on March 6, 2020.

[2] C. Countryman, "The fire environment concept", in *USDA For. Serv., Pac. Southwest For. and Range Exp. Station.*, 1972, 15 p.

[3] A. Tomas, C. Andrés, C. Ana, M. Tomas, "Time aware genetic algorithm fire propagation prediction: exploiting multi-core platforms", *Concurr. Comput.* **29** (2017), p. 1-18.

[4] O. Rios, M. Valero, E. Pastor, E. Planas, "A data-driven fire spread simulator: Validation in Vall-llobrega's fire", *Front. Mech. Eng.* **5** (2019), p. 1-11.

[5] M. Rochoux, C. Emery, S. Ricci, B. Cuenot, A. Trouvé, "A comparative study of parameter estimation and state estimation approaches in data - driven wildfire spread modeling", in *VII International Conference on Forest Fire Research, Coimbra*, 2014, p. 1-12.

[6] A. Farguell, A. Cortés, T. Margalef, J. Miro, J. Mercader, "Data resolution effects on a coupled data driven system for forest fire propagation prediction", *Procedia Comput. Sci.* **108** (2017), p. 1562-1571.

[7] Y. Xin-She, K. Slawomir, *Computational Optimization and Applications in Engineering and Industry*, vol. 356, Springer, Berlin, Heidelberg, 2011, 1-11 pages.

[8] M. H. Tchiekre, A. D. V. Brou, J. K. Adou, "Detreministic optimization techniques to calibrate parameters in a wildland fire propagation model", *C. R. Méc.* **348** (2020), p. 759-768.

[9] B. Porterie, N. Zekri, J.-P. Clerc, J.-C. Loraud, "Un Réseau de Petit Monde local à sites pondérés pour les feux de forêts", *C. R. Phys.* **6** (2005), p. 151-157.

[10] B. Porterie, N. Zekri, J.-P. Clerc, J.-C. Loraud, "Influence des brandons sur la propagation d'un feu de forêt", *C. R. Phys.* **6** (2005), p. 1153-1160.

[11] A. Kaiss, L. Zekri, N. Zekri, B. Porterie, J.-P. Clerc, C. Picard, "Efficacité des coupures de combustible dans la prévention des feux de forêts", *C. R. Phys.* **8** (2007), p. 462-468.

[12] B. Porterie, N. Zekri, J.-P. Clerc, J.-P. Loraud, "Modeling forest fire spread and spotting process with small world networks", *Combust. Flame* **149** (2007), p. 63-78.

[13] J. Adou, Y. Billaud, D. Brou, J.-P. Clerc, J.-L. Consalvi, A. Fuentes, A. Kaiss, F. Nmira, B. Porterie, L. Zekri, N. Zekri, "Simulating wildfire patterns using a small - world network model", *Ecol. Model.* **221** (2010), p. 1463-1471.

[14] J. Adou, A. Brou, B. Porterie, "Modeling wildland fire propagation using a semi - physical network model", *Case Stud. Fire Saf.* **4** (2015), p. 11-18.

[15] Gouvernement de Côte d'Ivoire, "Portail Officiel du Gouvernement de Côte d'Ivoire", Available at: http://www.gouv.ci/_actualite-article.php?d=3&recordID=8535. Accessed on April 23, 2020.

[16] B. Monod, A. Collin, G. Parent, P. Boulet, "Infrared radiative properties of vegetation involved in forest fires", *Fire Saf. J.* **44** (2009), p. 88-95.

[17] Z. Acem, G. Parent, B. Monod, G. Jeandel, P. Boulet, "Experiment study in the infrared of the radiative properties of pine needles", *Exp. Therm. Fluid Sci.* **34** (2010), p. 893-899.

[18] F. M. White, *Heat and Mass Transfer*, Addison-Wesley, Reading, MA, 1988, Ed., 2, illustrated, reprinted, 718 pages.

[19] M. B. Kenneth, W. R. Kenneth, J. R. Christopher, "Modeling thermally thick pyrolysis of wood", *Biomass Bioenerg.* **22** (2002), p. 41-53.

[20] B. Babu, A. S. Chaurasia, "Heat transfert and kinetics in the pyrolysis of shrinking biomass particle", *Chem. Eng. Sci.* **59** (2004), p. 1999-2012.

[21] Z. Kuo, S. José, G. Daniel, M. German, F. Gilles, "Modeling of beech wood pellet pyrolisis under concentrated solar radiation", *Renew. Energ.* **99** (2006), p. 721-729.

[22] E. Grieco, G. Baldi, "Analysis and modelling of wood pyrolysis", *Chem. Eng. Sci.* **66** (2011), p. 650-660.

[23] X. Sànchez-Monroy, W. Mell, J. Torres-Arenas, B. W. Butler, "Fire spread upslope: Numerical simulation of laboratory esperiments", *Fire Saf. J.* **108** (2019), article no. 102844.

[24] Scilab Company, (Addressed 04/11/2019), http://www.scilab.org.

[25] A. B. N'Dri, D. S. Tionhonkélé, G. Jacques, D. Kanvaly, K. Mouhamadou, K. N. Julien, A. K. N'golo, B. Sébastien, "Season affects fire behavior in annually burned humid savanna of West Africa", *Fire Ecol.* **14** (2018), p. 1-11.